RSC Advances

PAPER

View Article Online
View Journal | View Issue

Cite this: *RSC Adv.*, 2022, **12**, 36158

Degradation of pyrene in contaminated soil by the dielectric barrier discharge combined with the $MnFe_2O_4$ catalyst†

Zixu Zeng,[a] Yani Zhang,[a] Xianlun Xu,[a] Shaoyun Hao,[a] Lecheng Lei[ab] and Xingwang Zhang *[ab]

Received 5th October 2022
Accepted 27th November 2022

DOI: 10.1039/d2ra06251h

rsc.li/rsc-advances

In this work, a spinel oxide of $MnFe_2O_4$ was used as the dielectric barrier discharge (DBD) catalyst for the remediation of pyrene-contaminated soil. The performances were investigated through tuning voltage, frequency, catalyst dosage, and soil moisture. Under the optimal conditions, such as the voltage of 10.0 kV, the discharge frequency of 1.0 kHz, $MnFe_2O_4$ dosage of 0.3 g, air flow rate of 2.0 L min^{-1}, soil humidity of 5.3%, and degradation efficiency of DBD/$MnFe_2O_4$ for pyrene could reach 79.26% after 10 min treatment, which was much higher than that of DBD for pyrene of 42.56%. The DBD/$MnFe_2O_4$ system also showed the high degradation efficiency of other pollutants including phenanthrene, *p*-nitrophenol, and *p*-nitrophenol in contaminated soil. The enhancing mechanism of the DBD/$MnFe_2O_4$ system was discussed.

Introduction

Organic contaminated soils have attracted widespread attention around the world. Many refractory organic pollutants, such as polycyclic aromatic hydrocarbons, organochlorine pesticides, and polychlorinated biphenyls, are environmentally persistent and have bioaccumulate property, long-distance mobility, and high toxicity.[1] The organic pollutants are firstly absorbed by the rhizomes of plants, then come in the food chain, and finally enter the human body through transfer, posing a serious threat to human health.[2–4] Consequently, it is obviously of significance to deal with the degradation of these persistent organic pollutants in soil.

For these refractory organic pollutants in soil, we often use thermal desorption,[5] stream vapor extraction,[6] and soil washing technology[7] as physical methods to remove organic pollutants in soil with high soil remediation efficiency, but these physical remediation methods need high energy consumption and the pollutants need further treatment. Besides, chemical oxidation technology,[8] ozone oxidation technology,[9] and advanced oxidation process[10] are also used for the degradation of organic pollutants in soil. Wang *et al.*[8] used titanium dioxide (P25) as the photocatalyst to degrade diphenylarsinic acid. Flotron *et al.*[10] applied Fenton reaction to treat the PAHs in soil and investigated the competitive effect among PAHs during degradation. The chemical methods have simple processing steps but people have to consider how to deal with the secondary pollution. In addition, bioremediation technologies of microbial remediation technology,[11] phytoremediation technology, and fauna remediation technology are mild to the environment but they cost too much time during soil recovery.

Dielectric barrier discharge (DBD) is a promising advanced oxidation process method with little secondary pollution. DBD can generate high-energy electrons through high-voltage discharge and break the chemical structure of gas molecules in the air (*e.g.* O_2); besides, DBD can also generate physical effects such as UV and chemically active substances including free radicals (·OH, $\cdot HO_2$), high-energy electrons, OH–, and ozone (O_3).[12,13] These physical effects and chemical substances can degrade many pollutants in water or soil, causing them to degrade into lower molecular weight products or less harmful products, such as H_2O and CO_2.[14,15] Redolfi *et al.*[16] used DBD to remediate soil contaminated with kerosene, and the degradation efficiency of kerosene reached 88% after 12 min of treatment. Aggelopoulos *et al.*[14] studied the remediation of non-aqueous phase liquid-contaminated soil simulated composite contaminated soil with DBD, and they calculated that the energy density was 6750 J g^{-1} for the soil. Mu *et al.*[17] investigated that the degradation efficiency of pyrene was influenced by soil pH to a certain extent, and the pyrene removal rate reached 68% under specified conditions. Although DBD is a promising method for the treatment of organic contaminated soils, UV light and ozone produced in DBD do not possess high oxidant capacity to effectively degrade pollutants.[14,17] To be more specific, on exposure to UV light and ozone, the coupling of

[a]*Key Laboratory of Biomass Chemical Engineering of Ministry of Education, College of Chemical and Biological Engineering, Zhejiang University, Hangzhou, 310027, China. E-mail: xwzhang@zju.edu.cn*

[b]*Institute of Zhejiang University-Quzhou, Weier Road, Quzhou, 324000, China*

† Electronic supplementary information (ESI) available. See DOI: https://doi.org/10.1039/d2ra06251h

catalysts with DBD can produce more active ·OH to improve the degradation efficiency of pollutants.[18,19] The research on using DBD to remediate polluted soil is in the initial stage, and it has not been applied to large-scale industrialization yet. Therefore, more experiments should be carried out to further explore its coupling effect between DBD and new catalysts to increase the removal efficiency of pollutants in soil.

Spinel oxide is a kind of metal oxide with a composition of AB_2O_4, where A^{2+} is the divalent metal cation, B^{3+} is the trivalent metal cation, and O^{2-} is the divalent oxygen anion. Spinel oxides have a cubic symmetric $Fd\bar{3}m$ space group,[20] which has $8A^{2+}$, $16B^{3+}$, and $32O^{2-}$, of which $32O^{2-}$ constitute face-centered cube, and $8A^{2+}$ and $16B^{3+}$ are filled in the voids of the face-centered cube in a tetrahedral structure and an octahedral structure, respectively.[21] The complex unit cell composition of spinel oxides endows it with a great number of oxygen vacancies, which can promote the transfer between cations and contribute to the application of spinel oxides in many catalytic reactions,[22] such as ozonation[23] and photocatalysis.[24] Mehandjiev *et al.*[23] studied the catalytic activities of the spinel oxide of $NiMn_2O_4$ under the situation of ozone-catalytic oxidation of benzene at low temperatures, and they found that the catalyst activity would be higher and the catalyst would be more stable when the two metal cations are located in octahedral coordination. As we know, there are ozone, UV light *etc.*, in DBD; thus, the introduction of spinel oxide catalyst to DBD will be expected to improve the degradation efficiency of the pollutant.

In this study, the spinel oxide of $MnFe_2O_4$ was synthesized by the hydrothermal method, and a DBD/$MnFe_2O_4$ catalytic system was constructed and used to remediate the pyrene-contaminated soil with the aim of improving the degradation efficiency of pollutants. The morphology, structure, and composition of the prepared $MnFe_2O_4$ were carefully characterized. The degradation efficiency of pyrene and the energy efficiency under different reaction conditions were optimized. The enhancing mechanism of the DBD/$MnFe_2O_4$ system was discussed.

Experimental

Experimental system

Fig. 1 shows the experimental system. This system was fully composed of pulsed high voltage power supply, monitoring system, and discharge reactor. In this reactor, the high-voltage electrode was connected to the pulsed high-voltage power supply, connected in parallel with the high-voltage probe, the low-voltage electrode was grounded, and was connected in series with the current probe. Besides, the electrical parameters were recorded by an oscilloscope. The soil was uniformly placed in the discharge area.

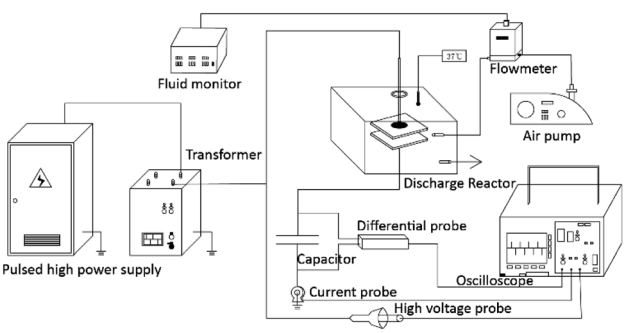

Fig. 1 Flow chart of the experiments.

Chemicals and equipment

Pyrene (Pye 97%), phenanthrene (PHE 95%), *p*-nitrophenol (PNP AR), methanol (99.9%), manganese nitrate (AR), ferric nitrate (AR), and sodium hydroxide (AR) were supplied by Sinopharm Chemical Reagent Co., Ltd.

High-voltage pulse power supply (KPF-II-5 A/25 kV, Jinhua Environmental Protection Technology Co., Ltd), oscilloscope (DPO4054B, Tektronix, USA), high-voltage probe (PVM-5, North Star, USA), current probe (6586, Pearson Electronics, USA), differential probe (SI-9002, Sapphire Instruments), and high-performance liquid chromatography (HPLC, 1260, Agilent Technology Co., Ltd, USA).

Catalyst preparation

The spinel oxides were synthesized by the hydrothermal method. Manganese nitrate ($Mn(NO_3)_2$) and ferric nitrate ($Fe(NO_3)_3$) were selected to synthesize $MnFe_2O_4$, respectively. The starting materials of manganese nitrate (0.1 M) and ferric nitrate (0.2 M) were mixed with 100 mL deionized water. The solution was co-precipitated with proper NaOH. All these operations were performed in a water bath at 90 °C under magnetic stirring at 1000 rpm. The mixture was transferred into a 250 L high-pressure tempering reactor and reacted at 140 °C for 12 hours. After the reaction, the as-prepared products were washed with distilled water and ethanol several times. In the end, the as-prepared products were dried for 12 hours at 70 °C.

Characterization

Scanning electron microscopy (SEM, Hitachi SU-70) combined with energy dispersive spectrometry (EDS) was used to characterize the morphology and elements of the sample. X-ray diffractometer (XRD) was used to analyze the crystal structure of the sample. The composition, content, and valence state of chemical elements in the samples were analyzed by X-ray photoelectron spectroscopy (XPS, Thermo Scientific K-Alpha).

Degradation experiments

Preparation of pyrene-contaminated soil: 500 g soil was weighed into a 1.0 L beaker. 1000 mL of 1000 mg L^{-1} methanol solution of pyrene was added to the beaker and stirred mechanically at 350 rpm min^{-1} for 6.0 h. After that, the mixture was transferred to a fume cupboard and stirred at 350 rpm min^{-1} until most of the methanol was evaporated. The soil was then transferred to a tray in a fume cupboard and dried at 70 °C for several days. For the batch experiment, the soil contaminated by organic pollutants is put on homogeneously on the ground electrode. The soil moisture was adjusted to obtain the soil samples for

experiments. After setting the voltages and pulse frequencies, the DBD process for the treatment of soil starts. After treatment, the soil was collected and analyzed. It should be noted that the operator needed training for the use of a high voltage power.

Preparation of the catalyst-contaminated soil: a certain quality of pyrene-contaminated soil was weighed, mixed evenly with 0.1–0.4 g catalysts, and placed it on the low-voltage electrode of the reactor.

Degradation experiment: under aeration conditions, pulse low-temperature plasma discharge treatment was performed; soil samples at different times were taken for residual concentration.

Contaminant extraction and analysis

Methanol acts as the extractant, the soil to be tested was placed in a 50 mL centrifuge tube, sonicated for 30 min, centrifuged at 10 000 rpm for 5 min, and the supernatant was taken out through a 0.22 μm filter membrane and placed in a sample bottle.

The quantitative analysis of pyrene was conducted by high-performance liquid chromatography. The determination conditions were as follows: UV detector, C18 column (4.6 × 250 mm, 5 μm), methanol/water 90/10, flow rate 0.8 mL min^{-1}, column temperature 40 °C, and wavelength 270 nm.

Pyrene and its by-products were identified by HPLC-MS (HPLC-MS, Acquity TM ultra/Triple TOF 5600+, Waters/AB SCIEX). Mass spectrometry conditions: UPLC-Triple-TOF 5600 + time-of-flight liquid chromatography and mass spectrometry, with positive and negative ion scan mode and its scan range: *m*/*z* 100–1500, with nebulizer gas (GS1, GS2): 55 psi and Curtain Gas (CUR): 35 psi, with Ion Source Temperature (TEM): 600 °C (positive) and 550 °C (negative), with Ion Source Voltage (IS): −4500 V (negative) and 5500 V (positive), with secondary scan of Declustering Potential (DP): 100 V, with focusing potential (CE): 10 V, with secondary scan that the MS data is collected using the TOF MS-Product Ion-IDA mode, CID energy 40 ± 20 eV, and using the CDS pump to do mass axis correction before injection, so that the mass axis error is less than the level of mg kg^{-1}.

The degradation efficiency and energy utilization efficiency are calculated with eqn (S1–S4) shown in ESI.†

Results and discussion

Catalyst characterization

The morphology and structure of $MnFe_2O_4$ catalysts were analyzed, as shown in Fig. 2. It can be seen from Fig. 2 that the prepared $MnFe_2O_4$ is granular and the particle size of $MnFe_2O_4$ is about 200–300 nm, as shown in Fig. 2a and b. To further analyze the elemental composition of $MnFe_2O_4$, energy dispersive spectrometer (EDS) analysis was carried out, and the results are shown in Fig. 2c and Table S1.† The results implied that the catalyst contained Mn, Fe, and O, and the atomic percentages of the elements were 17.22%, 32.62%, and 50.16%, respectively. The element ratio of Mn and Fe is similar with the ratio of the metal elements added during the preparation of the catalyst, confirming the spinel oxide structure of $MnFe_2O_4$.

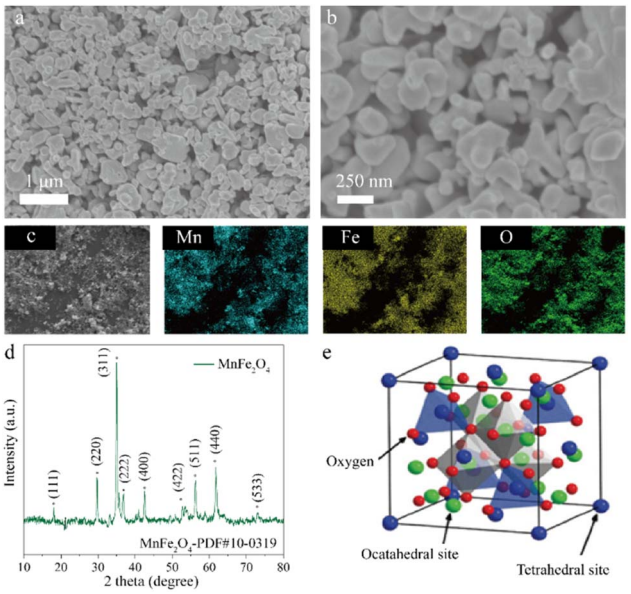

Fig. 2 Characterization of $MnFe_2O_4$. (a) SEM image of $MnFe_2O_4$. (b) SEM image of $MnFe_2O_4$-60 k. (c) Elemental mapping. (d) XRD pattern for $MnFe_2O_4$. (e) The spinel oxide crystal structure.

The crystal structure of $MnFe_2O_4$ was further determined by XRD; the results are shown in Fig. 2d. It could be found that the three strongest diffraction peaks correspond to the (311), (220), and (440) planes of $MnFe_2O_4$, respectively (PDF #10-0319). The other strong diffraction peaks, such as those for (111), (220), (222), (400), and (511), also matched with the peaks of $MnFe_2O_4$.

The chemical valence and state of $MnFe_2O_4$ were characterized, as shown in Fig. 3. In Fig. 3b, the Mn 2p spectrum for $MnFe_2O_4$ is shown, with the peaks at 641.43 eV and 653.1 eV corresponding to Mn $2p_{3/2}$ and Mn $2p_{1/2}$, respectively.[25] In Fig. 3c, for the spectrum of Fe 2p in $MnFe_2O_4$, the curve could be

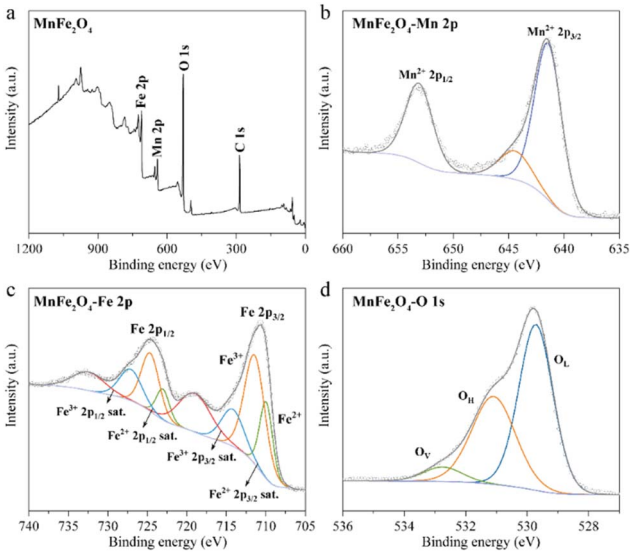

Fig. 3 XPS of $MnFe_2O_4$. (a) XPS survey pattern. XPS spectra of Mn 2p (b), Fe 2p (c), and O 1s (d).

fitted to two main peaks of Fe $2p_{3/2}$ and Fe $2p_{1/2}$ and their corresponding two satellite peaks. The peak value of Fe $2p_{3/2}$ is 711.41 eV, and the peak value of Fe $2p_{1/2}$ is 724.63 eV. Their satellite peaks were 718.98 eV and 732.44 eV, respectively. Among them, the mass fractions of Fe^{2+} and Fe^{3+} were 30.83% and 69.17%,[26] respectively, indicating that the Fe elements in $MnFe_2O_4$ exist in the +3 state, and the transition of the valence state of the two elements, Fe^{3+} to Fe^{2+}, indirectly proving that the oxygen vacancies were introduced into the lattice. These oxygen vacancies are important active sites for catalyzing ozone oxidation,[27,28] which is consistent with the M–K reaction mechanism. Fig. 3d shows the O 1s of $MnFe_2O_4$; the peaks at 529.71 eV and 531.09 eV binding energy correspond to lattice oxygen and adsorbed oxygen, respectively. Fig. S2† proved that the $MnFe_2O_4$ catalyst could be strongly attracted by a magnet, which means that it can be easily absorbed by the magnetic force.

Optimizing conditions of the DBD/$MnFe_2O_4$ system

To optimize the conditions of the DBD/$MnFe_2O_4$ system, we set the voltage, frequency, catalyst dosage, and soil moisture as the four key parameters to increase the degradation efficiency of pyrene. Besides, all the samples below have been treated by pulse low-temperature plasma discharge method under different aeration conditions. To be more specific, the fixed conditions of the discharge voltage (V), discharge frequency (f), air flow rate (r), soil pH, catalyst dosage (m), soil moisture (w), and discharge time (t) were $V = 10.0$ kV, $f = 1.0$ kHz, $r = 2.0$ L min^{-1}, pH = 7.3, $m = 0.3$ g, $w = 3.0\%$, and $t = 10$ min.

During the DBD process, the active species could be generated and accompanied by the occurrence of physical effects such as light,[29] heat,[30] and UV light.[31] These effects are closely related to the discharge voltage; thus, increasing the discharge voltage can also enhance the above effects.[29,31,32] As shown in Fig. 4, we can come to the conclusion that with the increase in voltage, the degradation efficiency of pyrene also increases. Fig. 4 has also confirmed that the DBD/$MnFe_2O_4$ system can effectively improve the degradation efficiency of pyrene compared with the DBD system without any catalyst at different voltages.

We systematically investigated the effect of discharging voltage on the pyrene-contaminated soil degradation by the DBD system. The degradation efficiency of pyrene was measured at 0.0 kV, 11.4 kV, 12.0 kV, and 13.1 kV, and the corresponding results are shown in Fig. 4. Fig. 4 shows that since the voltage increased from 10.0 kV to 13.1 kV, the degradation efficiency of pyrene increased by 26.98% without the catalyst and 15.85% with the catalyst, which indicated that increasing the discharge voltage could improve the degradation efficiency of pyrene. Moreover, the degradation efficiency of pyrene increased from 49.55% to 69.28% at 10 kV and from 77.52% to 85.13% at 13.1 kV. With the addition of $MnFe_2O_4$ catalyst, the increase in the degradation efficiency is more noteworthy under low voltage.

To study the effect of different frequencies on the degradation of pyrene-contaminated soil by the DBD system synergistically with $MnFe_2O_4$, the pyrene degradation efficiency was measured at 1.0 kHz, 1.2 kHz, 1.4 kHz, and 2.0 kHz. The corresponding results are shown in Fig. 5. It was shown that when the frequency was increased from 1.0 kHz to 2.0 kHz, the pyrene degradation efficiency increased by 8.91% and 7.78%, respectively, which indicated that raising the discharge frequency could ameliorate the pyrene degradation efficiency. However, when the discharge frequency rose from 1.0 kHz to 2.0 kHz, the power of the reactor was also raised from 1.84 W to 3.68 W. Considering the economic benefits,[33] 1.0 kHz was chosen as the discharge frequency.

To investigate the effect of catalyst dosage on the degradation of pyrene-contaminated soil by the DBD system, catalyst dosages of 0.1 g, 0.2 g, 0.3 g, and 0.4 g were applied to test the pyrene degradation efficiency, respectively. The corresponding results are shown in Fig. 6, which indicates that continuously

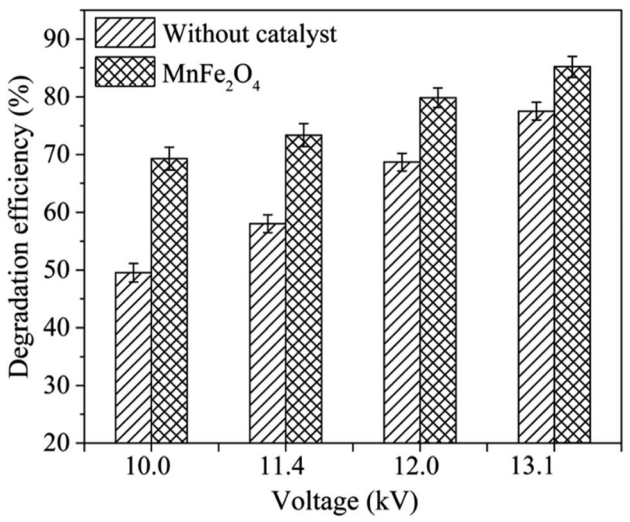

Fig. 4 Effect of different discharging voltages on the pyrene degradation efficiency.

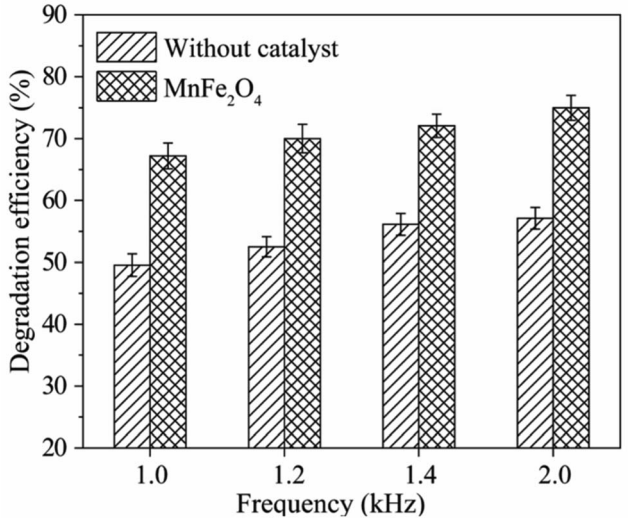

Fig. 5 Effect of different frequencies on the pyrene degradation efficiency.

increasing the amount of $MnFe_2O_4$ can gradually improve the pyrene degradation efficiency. As the catalyst dosage was increased from 0.1 g to 0.4 g, the degradation efficiency of pyrene was increased from 45.90% to 69.69%, which could explain why the gradual increase in the catalyst dosage increased the number of active sites in the reaction area, thereby generating more active species such as ·OH. As the amount of $MnFe_2O_4$ increases, it will occupy part of the discharge space, resulting in a decrease in the input energy, thus affecting the degradation efficiency of pyrene. To be more efficiency, we choose 0.3 g as the catalyst dosage.

To investigate the effect of soil moisture on the degradation of pyrene-contaminated soil by the DBD system, the pyrene degradation efficiency was determined with soil moisture of 0%, 3.0%, 5.3%, and 8.3%, respectively. The results are shown in Fig. 7, which indicates that increasing the soil moisture content within a certain range can significantly ameliorate the pyrene degradation efficiency. When the soil moisture content is 5.3%, the DBD/$MnFe_2O_4$ system shows the highest degradation efficiency of pyrene, reaching 79.26% from 42.56% without $MnFe_2O_4$. This is because catalysts are excited to generate more electrons and more vacancies so that the water in soil can react with catalysts more easily to generate more ·OH.[16,34] In the end, the pyrene degradation efficiency increases greatly. To be more specific, under neutral and basic conditions, surface hydroxyl groups are formed on the catalyst surface, which then transform into ·OH with O_3,[28] as shown in eqn (1) and (2). In addition, too much water will contribute to the accumulation of soil, which will affect the diffusion of protons and lower the degradation efficiency. In brief, 5.3% soil moisture was considered to be optimum.

$$S + H_2O \rightarrow HO\text{–}S + H_2 \quad (1)$$

$$HO\text{–}S + O_3 \rightarrow O_3\text{–}S + \cdot OH \quad (2)$$

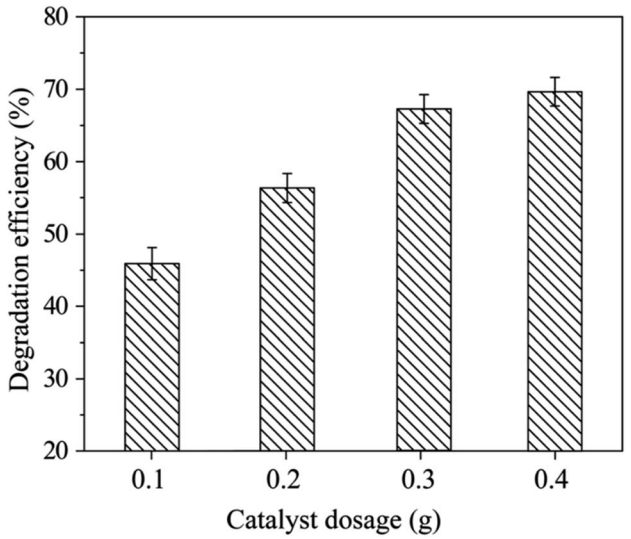

Fig. 6 Effect of catalyst dosage on the degradation efficiency of pyrene.

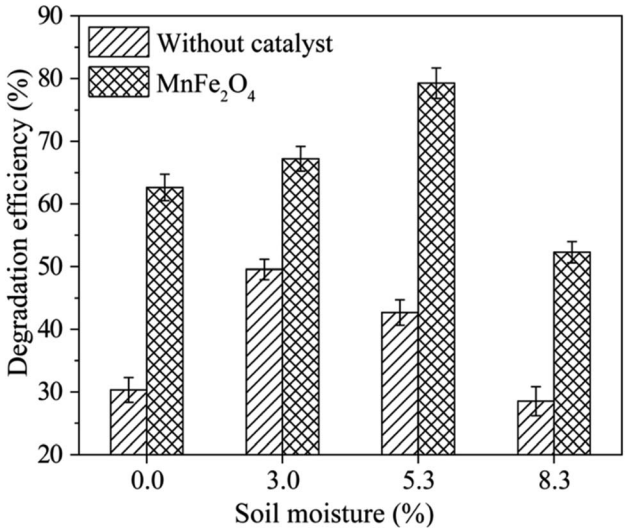

Fig. 7 Effect of soil moisture on pyrene degradation.

DBD/$MnFe_2O_4$ applied to other pollutants' degradation

We used the DBD/$MnFe_2O_4$ system to treat other typical organic pollutants including phenanthrene, *p*-nitrophenol, and pyrene-*p*-nitrophenol contaminated soil, respectively; the results are shown in Fig. 8. Both the treatments are the same to the fixed condition in the above Fig. 4–7, with $V = 10.0$ kV, $f = 1.0$ kHz, $r = 2.0$ L min^{-1}, pH = 7.3, $m = 0.3$ g, $w = 3.0\%$. The results show that the DBD/$MnFe_2O_4$ system has a good remediation effect on other organic polluted soils and can degrade most of the pollutants in a short time, indicating which one is more active than DBD.

We also investigated the influence of pH on pyrene degradation (Fig. S3†). Under neutral and basic conditions, surface hydroxyl groups are formed on the catalyst surface and transformed into ·OH with O_3,[28,33] showing higher degradation efficiency.

Enhancing mechanism

The above results clearly showed that the introduction of $MnFe_2O_4$ into DBD enhanced the degradation efficiency of pollutants in soil. The enhanced degradation effect of the DBD/$MnFe_2O_4$ system process are possibly attributed to several combining factors: (1) ozone in DBD can react with the surface hydroxyl groups of $MnFe_2O_4$ catalysts to form ·OH;[34] (2) the UV produced during DBD can accelerate the reaction on $MnFe_2O_4$

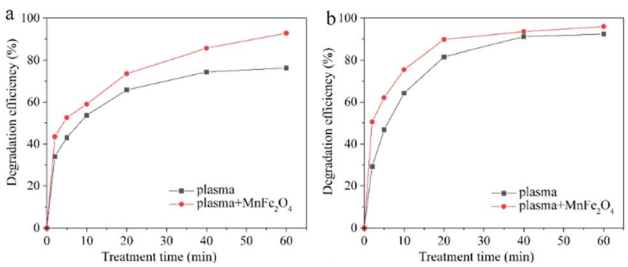

Fig. 8 The DBD/$MnFe_2O_4$ system for other pollutants' degradation. (a) Phenanthrene; (b) *p*-nitrophenol.

forming ·OH;[31] (3) proper soil moisture can provide a better environment for maintaining O_3 and producing ·OH.[16,34] More ·OH resulted in a higher degradation efficiency of the pollutants of the DBD/$MnFe_2O_4$ system.

Conclusion

In this study, the DBD/$MnFe_2O_4$ catalytic system was constructed for the effective remediation of contaminated soil. The DBD/$MnFe_2O_4$ system exhibited much higher degradation efficiency for pollutants than that of DBD. In view of the conditions of voltage of 10.0 kV, frequency of 1.0 kHz, catalyst dosage of 0.3 g, air flow rate of 2.0 L min^{-1}, and soil moisture of 5.3%, the pyrene degradation efficiency could reach 79.26% in the DBD/$MnFe_2O_4$ system. Compared with the pure DBD system, the degradation efficiency of DBD/$MnFe_2O_4$ for pyrene could increase by 36.70%. It was concluded that the addition of the $MnFe_2O_4$ catalyst can effectively improve the degradation efficiency of pyrene. The enhancing mechanism of the DBD/$MnFe_2O_4$ system for the remediation of pyrene-contaminated soil has also been discussed.

Author contributions

Zixu Zeng and Xianlun Xu: conceptualization, methodology, visualization, investigation. Zixu Zeng: formal analysis, writing-original draft preparation. Yani Zhang, Shaoyun Hao: project administration, writing-reviewing and editing. Xingwang Zhang and Lecheng Lei: supervision, project administration, funding acquisition.

Conflicts of interest

There are no conflicts to declare.

Acknowledgements

This study was supported by the National Key Research and Development Program of China (Project No. 2019YFC1805602).

Notes and references

1 J. Sun, L. Pan, Y. Zhan, H. Lu, D. C. W. Tsang, W. Liu, X. Wang, X. Li and L. Zhu, *Sci. Total Environ.*, 2016, **544**, 670–676.
2 S. Dudka and W. P. Miller, *J. Environ. Sci. Health, Part B*, 1999, **34**, 681–708.
3 Y. Liu, S. Li, Z. Ni, M. Qu, D. Zhong, C. Ye and F. Tang, *Sci. Total Environ.*, 2016, **542**, 620–628.
4 Y. Chen, J. Zhang, Q. Ma, C. Sun, S. Ha and F. Zhang, *Hum. Ecol. Risk Assess.*, 2016, **22**, 706–720.
5 C. Zhao, Y. Dong, Y. Feng, Y. Li and Y. Dong, *Chemosphere*, 2019, **221**, 841–855.
6 A. A. Soares, J. T. Albergaria, V. F. Domingues, M. da C. M. Alvim-Ferraz and C. Delerue-Matos, *Chemosphere*, 2010, **80**, 823–828.
7 G. Dermont, M. Bergeron, G. Mercier and M. Richer-Laflèche, *J. Hazard. Mater.*, 2008, **152**, 1–31.
8 A. Wang, Y. Teng, X. Hu, L. Wu, Y. Huang, Y. Luo and P. Christie, *Sci. Total Environ.*, 2016, **541**, 348–355.
9 M. M. Huber, S. Canonica, G.-Y. Park and U. von Gunten, *Environ. Sci. Technol.*, 2003, **37**, 1016–1024.
10 V. Flotron, C. Delteil, Y. Padellec and V. Camel, *Chemosphere*, 2005, **59**, 1427–1437.
11 J. Wang, X. Zhang and G. Li, *J. Soils Sediments*, 2012, **12**, 117–127.
12 H. Shao and X. Li, *J. Alloys Compd.*, 2016, **667**, 191–197.
13 S. Y. Liu, D. H. Mei, Z. Shen and X. Tu, *J. Phys. Chem. C*, 2014, **118**, 10686–10693.
14 C. A. Aggelopoulos, C. D. Tsakiroglou, S. Ognier and S. Cavadias, *Int. J. Environ. Sci. Technol.*, 2015, **12**, 1011–1020.
15 J.-S. Chang, P. A. Lawless and T. Yamamoto, *IEEE Trans. Plasma Sci.*, 1991, **19**, 1152–1166.
16 M. Redolfi, C. Makhloufi, S. Ognier, S. Cavadias, D. Tzovolou and C. Tsakiroglou, *High Temp. Mater. Processes*, 2009, **13**, 427–437.
17 R. Mu, Y. Liu, R. Li, G. Xue and S. Ognier, *Chem. Eng. J.*, 2016, **296**, 356–365.
18 A. M. Vandenbroucke, M. Mora, C. Jiménez-Sanchidrián, F. J. Romero-Salguero, N. De Geyter, C. Leys and R. Morent, *Appl. Catal., B*, 2014, **156–157**, 94–100.
19 Z. Yao, L. Liu, X. Xiao, C. Wang, L. Jiang and L. Chen, *J. Alloys Compd.*, 2018, **731**, 524–530.
20 E. Gorter, *Philips Res. Rep.*, 1954, **9**, 403–443.
21 S. K. Gore, R. S. Mane, M. Naushad, S. S. Jadhav, M. K. Zate, Z. A. Alothman and B. K. N. Hui, *Dalton Trans.*, 2015, **44**, 6384–6390.
22 F. Qi, B. Xu and W. Chu, *J. Mol. Catal. A: Chem.*, 2015, **396**, 164–173.
23 D. Mehandjiev, A. Naydenov and G. Ivanov, *Appl. Catal., A*, 2001, **206**, 13–18.
24 V. S. Kirankumar and S. Sumathi, *Mater. Today Chem.*, 2020, **18**, 100355.
25 X. Wang, P. Xu, C. Yang, T. Shen, J. Qu, P. Wang and G. Zhang, *J. Hazard. Mater.*, 2021, **414**, 125602.
26 Y. Yao, Y. Cai, F. Lu, F. Wei, X. Wang and S. Wang, *J. Hazard. Mater.*, 2014, **270**, 61–70.
27 Y. Ding, L. Zhu, N. Wang and H. Tang, *Appl. Catal., B*, 2013, **129**, 153–162.
28 R. Zhang, Q. Zhong, W. Zhao, L. Yu and H. Qu, *Appl. Surf. Sci.*, 2014, **289**, 237–244.
29 P. Dong, F. Yang, X. Cheng, Z. Huang, X. Nie, Y. Xiao and X. Zhang, *Mater. Sci. Eng. C*, 2019, **96**, 197–204.
30 F. Rodrigues, J. Pascoa and M. Trancossi, *Exp. Therm. Fluid Sci.*, 2018, **90**, 55–65.
31 Y. Wei, G. Lu, D. Xie, T. Sun, Y. Liu, Y. Zhang, J. An, M. Li and H. Guo, *Chem. Eng. J.*, 2022, **431**, 133360.
32 N. Lu, J. Lou, C. H. Wang, J. Li and Y. Wu, *Water, Air, Soil Pollut.*, 2014, **225**, 1991.
33 N. Jiang, N. Lu, K. Shang, J. Li and Y. Wu, *J. Hazard. Mater.*, 2013, **262**, 387–393.
34 M. Ansari, A. Hossein Mahvi, M. Hossein Salmani, M. Sharifian, H. Fallahzadeh and M. Hassan Ehrampoush, *Sep. Purif. Technol.*, 2020, **251**, 117270.